

Diameter-Dependent Radial and Tangential Elastic Moduli of ZnO Nanowires

G. Stan,^{*,†} C. V. Ciobanu,^{*,‡} P. M. Parthangal,[§] and R. F. Cook[†]

Ceramics Division, National Institute of Standards and Technology, Gaithersburg, Maryland 20899, Division of Engineering, Colorado School of Mines, Golden, Colorado 80401, and Process Measurement Division, National Institute of Standards and Technology, Gaithersburg, Maryland 20899

Received August 9, 2007; Revised Manuscript Received October 11, 2007

ABSTRACT

We show how contact resonance atomic force microscopy (CR-AFM) can be used to accurately determine the radial elastic moduli of [0001] ZnO nanowires with diameters smaller than 150 nm. Using a realistic tip–nanowire contact geometry, we find the radial indentation modulus from CR-AFM data and the tangential shear modulus from friction-type measurements. Both moduli show a pronounced increase when the wire diameter is reduced below 80 nm. The size dependence of the elastic properties can be explained by a core–shell model that accounts for a bulk-like core and an elastically stiffer surface layer.

Zinc oxide nanostructures hold tremendous promise for novel and versatile devices due to their intrinsic semiconducting and piezoelectric properties, as well as the amazing structural diversity that can be achieved by current synthesis techniques.¹ ZnO nanostructures can take the form of nanowires, nanobelts, nanorings, and nanohelices,² with demonstrated potential for novel nanoscale piezoelectric devices.³ The ability to create such devices with predictable and reproducible operation depends, at least in part, on having knowledge of the structural and mechanical properties of ZnO nanostructures. The small dimensions of these nanostructures can, however, raise serious challenges for experimental investigations of properties relevant to device applications.

Current growth methods^{1,2} can yield ZnO nanowires (ZnO NWs) with diameters between 20 and 500 nm that are usually single-crystalline with the wurtzite structure and have the axis oriented along the [0001] direction. Tremendous and rapid progress has been achieved in synthesizing ZnO NWs, but experimental investigations of the nanomechanical properties and their size dependence have only recently been reported. In order to quantify the diameter dependence of the elastic properties of ZnO nanostructures, various techniques have been employed. For example, electric-field-induced resonance has been used with in situ transmission

electron microscopy (TEM) to measure the axial Young's modulus of ZnO NWs^{4,5} and nanobelts.⁶ Static and dynamic atomic force microscopy (AFM) and nanoindentation techniques have been used to measure the radial modulus,⁷ bending modulus,^{8,9} and buckling modulus¹⁰ of ZnO NWs and nanobelts. The elastic moduli reported so far span the range from 30 to 250 GPa and are often found to have no specific size dependence. However, in some experiments, a clear dependence of the Young's modulus of the nanowire diameter has been reported for ZnO NWs with diameters smaller than 150 nm.⁴ For nanobelts, the variation of the Young's modulus with the effective diameter of the cross section¹¹ and with the aspect ratio of the cross section has also been recently revealed.¹² The conflicting reports on Young's modulus and its dependence on wire diameter for ZnO NWs suggest a clear need for different and more accurate ways to measure the elastic properties of nanowires, with the immediate goal of elucidating the mechanical properties of ZnO NWs and, possibly, with the added benefit of applicability to NWs of other materials.

Here, we report on the size-dependent elasticity of ZnO nanowires using contact resonance atomic force microscopy (CR-AFM)¹³ and friction-type measurements.¹⁴ Our investigations complement current studies of elastic properties of ZnO NWs in several aspects. First, using CR-AFM, we determine the indentation modulus and the Young's modulus in the radial direction of ZnO NWs that are laid down on a substrate, whereas most other works have determined the axial modulus from measurements of the deflections of NWs

* To whom correspondence may be addressed. E-mail: gheorge.stan@nist.gov (G.S.); cciobanu@mines.edu (C.V.C.).

[†] Ceramics Division, National Institute of Standards and Technology.

[‡] Division of Engineering, Colorado School of Mines.

[§] Process Measurement Division, National Institute of Standards and Technology.

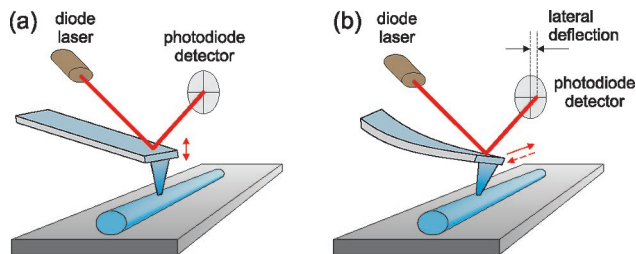


Figure 1. (a) Contact resonance atomic force microscopy (CR-AFM) experiments on a ZnO NW. The radial indentation modulus of the NW is determined from the change in resonance frequency that occurs when the probe tip is brought from air into contact with the wire. (b) Friction-type measurements on top of a nanowire. The lateral deflection, which is proportional to the lateral force on the cantilever, is used to determine the tangential shear modulus of the ZnO NW.

in various cantilever or suspended-beam configurations (e.g., ref 11). As such, the present work represents a versatile alternative to the current experimental paradigm¹⁵ for determining the mechanical properties of NWs, an alternative which is useful for NWs that are supported, formed, or bound longitudinally to a substrate. Second, we have employed a realistic sphere-on-cylinder geometry for the contact between the AFM probe tip and the nanowire. The contact geometry considered when extracting elastic properties from measured data turns out to be a key factor for accurate determinations of the elastic moduli of ZnO NWs with diameters that are comparable with the dimensions of the probe tip. Furthermore, in addition to the radial Young's modulus, we have also investigated another elastic property, the lateral shear modulus, which was determined from friction-type measurements. We have found that both the radial Young's modulus and the lateral shear modulus are strongly size dependent for diameters smaller than 80 nm, and we have rationalized this finding in terms of a core-shell model that accounts for a bulk core and a surface layer with different elastic moduli than those of the bulk.

Focusing first on the synthesis and characterization, we have grown ZnO NWs on Au catalyst layers deposited on SiO₂ substrates through thermal evaporation of commercial Zn powder at 550 °C in a N₂-O₂ gas mixture. The NWs were then cleaved from the substrate, suspended in ethanol, ultrasonicated, and dispersed on clean Si(111) wafers. Scanning electron microscopy (SEM) and AFM images of individual NWs before and after their removal from the substrate are shown in Figure 2a and 2b. High-resolution transmission electron microscopy (HRTEM) and electron diffraction analysis revealed that the ZnO NWs were single crystals grown along [0001] with an interplanar spacing of 2.55 ± 0.05 Å (Figure 2c), which corresponds to the known spacing between the adjacent (0002) planes of ZnO wurtzite. The SEM and the AFM imaging revealed smooth wires with lengths of several microns. Due to the growth procedure and conditions,¹⁶ the NWs had rounded cross sections¹⁷ (Figure 2a) rather than hexagonal ones.¹⁸ AFM profiles of the ZnO NWs were also consistent with circular cross sections, as seen in Figure 3a. The radius of the nanowire and that of the probe tip (approximated as a spherical surface) were

calculated by deconvoluting the contributions of the tip and the ZnO NW to the average cross-sectional AFM profile (Figure 3b).

An AFM (Veeco Multimode III, Santa Barbara, CA) was used to study the radial and tangential stiffnesses of the contact between an AFM probe (PPP-SEIH NanoSensors, Neuchatel, Switzerland)¹⁹ and the tested materials. The AFM probes were single-crystal Si cantilevers with integrated Si(100) tips. The spring constants k_c of the cantilevers were in the range of 8 < k_c < 12 Nm⁻¹, as determined from both the thermal-noise and the Sader methods.²⁰ For the CR-AFM measurements, a lock-in amplifier was used to induce vibrations in the cantilever and to collect the signal on the photodiode detector.²¹ The applied load of 250 nN, kept constant throughout the measurements, is much larger than the adhesion force while also small enough that the contact deformations are in the linear elastic regime. In this regime, the contact between the probe tip and the tested material behaves as a spring characterized by a contact stiffness that is specific to the direction of the movement of the tip (radial or lateral, refer to Figure 1). The mathematical framework necessary to extract elastic moduli from the measured contact stiffnesses is outlined below, with special focus on the geometry of the contact between the nanowire and the AFM tip.

To define the contact geometry, we approximate the probe tip as a spherical surface of radius R_T . The validity of this approximation has been confirmed by taking SEM images of the tip during the course of the measurements. In the classical Hertzian model,²² the contact area between the spherical tip and the cylindrical nanowire of radius R_{NW} is an ellipse of eccentricity e that can be calculated (numerically) from

$$\frac{R_{NW}}{R_T + R_{NW}} = (1 - e^2) \frac{K(e) - E(e)}{E(e) - (1 - e^2)K(e)} \quad (1)$$

where $K(e)$ and $E(e)$ are the complete elliptic integrals of first and second kind,²³ respectively. The major semiaxis a of the contact ellipse depends (in addition to R_T and R_{NW}) on the normal force P and the reduced elastic modulus E^* of the materials in contact, via

$$a = \frac{K(e)}{\pi} \left(\frac{6PR_T}{\gamma E^*} \right)^{1/3} \quad (2)$$

where $\gamma = 2(1 - e^2)K^3(e)(2R_{NW} + R_T)/\pi^2 E(e)R_{NW}$.²² In the isotropic approximation, the reduced elastic modulus E^* in eq 2 is defined as

$$\frac{1}{E^*} = \frac{1}{M_T} + \frac{1}{M_1} = \frac{1 - \nu_T^2}{E_T} + \frac{1 - \nu_1^2}{E_1} \quad (3)$$

where M_T , E_T , and ν_T are the indentation modulus, Young's modulus, and Poisson ratio of the tip and M_1 , E_1 , and ν_1 are the same quantities for the material with which the tip is brought in contact.

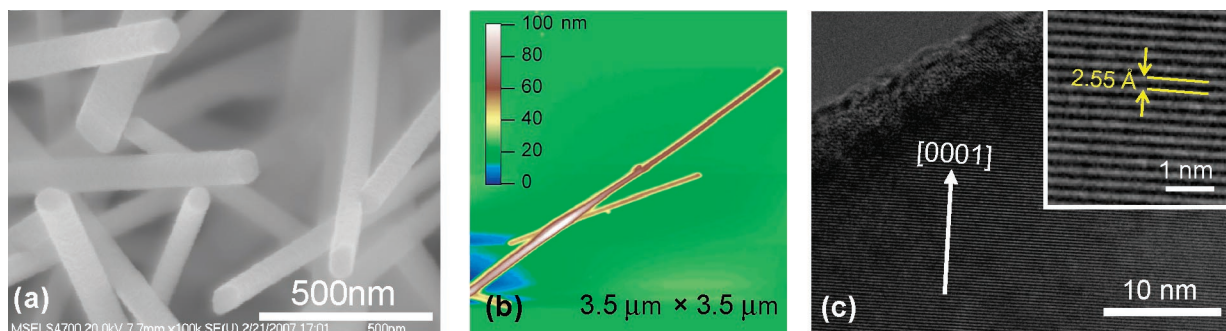


Figure 2. Morphological characterization of the ZnO NWs. (a) SEM image of as-grown nanowires. (b) AFM image of a nanowire that makes contact (parallel to its axis) with the Si(111) substrate. (c) HRTEM images of a ZnO NW showing the spatial periodicity of the (0002) atomic planes; the image was taken in the vicinity of a wire end and shows the presence of a polycrystalline surface layer (upper left corner). The inset shows a magnification of the (0002) planes, identifying the interplanar spacing of 2.55 Å.

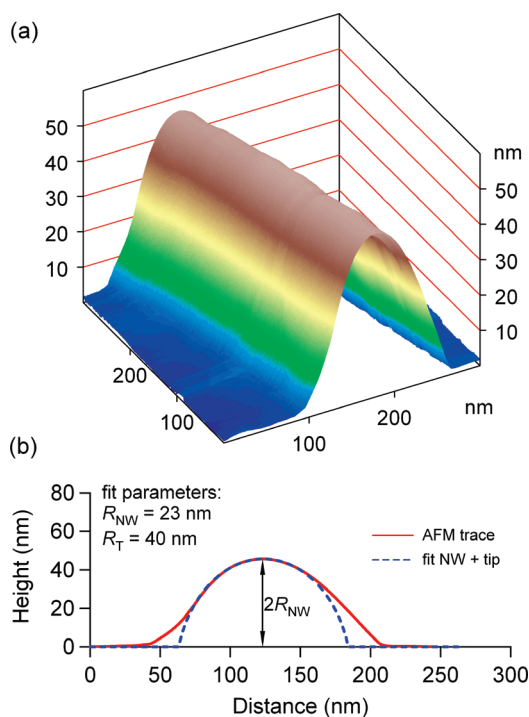


Figure 3. The contact between the probe tip and a 46 nm diameter ZnO NW. (a) Detailed AFM profile of a 300 nm segment of the nanowire. (b) Averaged cross section of the profile shown in panel (a), which is used to calculate the radius of the spherical AFM tip via an erosional fit of the cross section.

In the regime of small deformations, the contact can be described by a radial stiffness k^* defined as the derivative of the normal force P with respect to the change in the distance δ between the center of the sphere (tip) and the axis of the nanowire

$$k^* = \frac{\partial P}{\partial \delta} = \frac{\pi a E^*}{K(e)} \quad (4)$$

where $\delta = (9\gamma P^2/16R_T E^*)^{1/3}$ for the contact geometry considered. We perform contact stiffness measurements on a reference material (the Si(111) substrate, denoted by the subscript ref) and on the nanowire and then take the ratio $k_{\text{ref}}^*/k_{\text{NW}}^*$ in order to eliminate the force P that appears in

eq 4. Making use of eq 3 written separately for the probe contact with Si(111) and with a ZnO NW, we determined the radial indentation modulus M_{NW} of the nanowire from

$$\frac{1}{M_{\text{NW}}} = \gamma^{-1/2} \left(\frac{k_{\text{ref}}^*}{k_{\text{NW}}^*} \right)^{3/2} \left(\frac{1}{M_{\text{ref}}} + \frac{1}{M_T} \right) - \frac{1}{M_T} \quad (5)$$

where M_T and M_{ref} are the indentation moduli of the tip and the reference Si(111) substrate, respectively.²⁴

The ratio $k_{\text{ref}}^*/k_{\text{NW}}^*$ in eq 5 was calculated using CR-AFM measurements on each ZnO NW and on Si(111). In these measurements, the resonance frequency of the probe changes when it is brought from air into contact with a material, with the frequency shift determined by the geometry of the contact and the elastic properties of the materials involved. Figure 4a shows histograms of the lowest resonance frequency f_1 for contact with a 46 nm diameter NW and the Si(111) substrate. No significant change was detected in the resonance f_1 measured on the substrate before and after testing the ZnO NW, which confirms that the contact geometry is preserved during experiments, and thus the results are reproducible. With the resonance frequencies identified, the contact stiffness on each tested material was calculated using a clamped-coupled cantilever model system.¹³ We have expressed the lowest resonance frequencies f_1 and f_2 in terms of the fundamental resonance in air, f , and plotted them as functions of the stiffness ratio k^*/k_c (refer to Figure 4b). Once the curves f_1/f and f_2/f are fully determined by using the measured f_1 and f_2 values for the contact with Si(111), it is sufficient to measure just one resonance (e.g., f_1) for the contact with the ZnO NW, and the contact stiffness k^* can be found from the corresponding frequency curve. To verify that our contact stiffness determinations are reliable, we have measured both f_1 and f_2 for ZnO NWs and have found that both indeed give the same value for the contact stiffness k^* (see Figure 4b).

Before describing the results for the indentation modulus of ZnO NWs (eq 5), we briefly discuss the measurements used for determining the tangential shear modulus of the NWs. These are friction-type measurements¹⁴ performed with a nonvibrating probe tip dragged back and forth along the

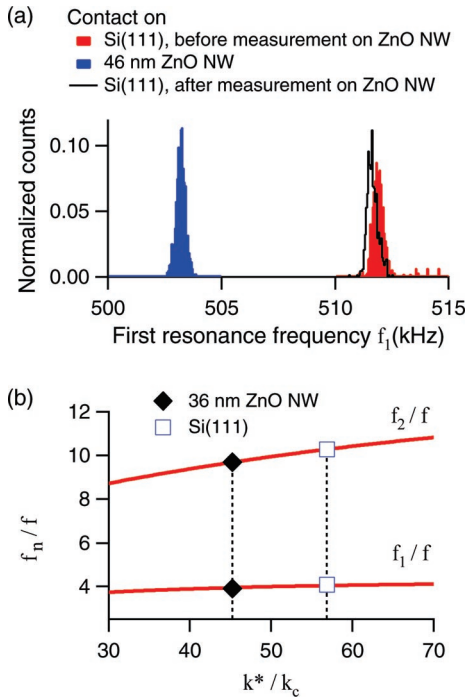


Figure 4. (a) Histograms of the first resonance frequency f_1 for an AFM probe on the Si(111) substrate (red), on a 46 nm diameter ZnO NW (blue), and again on the substrate (black). (b) Contact resonance frequencies f_1, f_2 (red curves) normalized to the fundamental resonance in air f and plotted as functions of the normalized contact stiffness k^*/k_c . These resonance frequencies depend on probe parameters that are determined by requiring that the experimental f_n/f ($n = 1, 2$) values for the contact with Si(111) lie on the corresponding curves. The contact stiffness k^* for any given nanowire can then be readily determined by using experimental values of the frequency ratios on either of the two curves, f_1/f or f_2/f .

surface of the nanowire (Figure 1b), with a speed of 10 nm s^{-1} and under a constant normal force of 250 nN. The lateral contact stiffness itself is characterized in the no-slip linear elastic regime. In this regime, the variation of the lateral force is proportional to the lateral voltage signal V from the photodiode (Figure 1b) and is recorded as a function of the displacement along the materials studied (Figure 5). The measurements yield the lateral stiffness κ , defined²⁹ as the change in lateral force F on the probe tip with displacement, $\kappa = \partial F/\partial d$. We express the lateral stiffness as $\kappa = \alpha s$, where α is a calibration coefficient that describes the proportionality between the lateral force and the deflection signal from the photodiode, and $s = \partial V/\partial d$ is the slope of the deflection curves (refer to Figure 5). As measured, κ includes¹⁴ not only a contribution κ^* from the contact between the tip and the material but also a contribution κ_p that comes from twisting the AFM probe

$$\frac{1}{\kappa} = \frac{1}{\kappa^*} + \frac{1}{\kappa_p} \quad (6)$$

The tangential shear modulus G_{NW} can be extracted from the measured lateral contact stiffness κ as described below.

Using again the Hertzian model,^{22,29} the lateral contact stiffness κ^* can be written in terms of lateral shear moduli

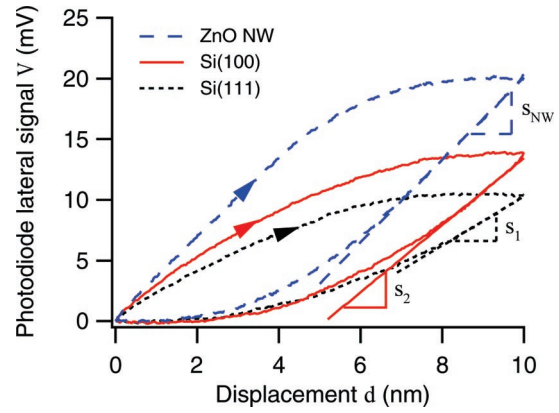


Figure 5. Lateral force-displacement curves measured on top of a 36 nm diameter ZnO NW (black curve), on Si(111) (blue), and on Si(100) (red). The arrows indicate the scan directions on the friction loops. The lateral force F in each case is proportional to the lateral signal V from the photodiode (refer to Figure 1b). Instead of working with an instrument-specific calibration between F and V , we determine and use lateral contact stiffnesses s_1, s_2 , and s_{NW} , that is, the slopes of the tangents to the friction loops in the linear no-slip regime.

G_T and G_{NW} of the two solids in contact, that is, the tip and the nanowire

$$\frac{1}{\kappa^*} = \frac{1}{2\pi a} \left[\frac{K(e) - \nu_T B(e)}{G_T} + \frac{K(e) - \nu_{NW} B(e)}{G_{NW}} \right] \quad (7)$$

where $B(e) = [E(e) - (1 - e^2)K(e)]/e^2$ and a is given by eq 2. Equation 6 contains two instrument-specific parameters α and κ_p , with the former requiring tedious calibration. However, these parameters can be eliminated by performing additional measurements on two reference materials, which we chose to be the Si(001) and Si(111) surfaces. Equations 6 and 7 (for the contact with the ZnO NW), in combination with their analogues for the measurements on the two reference surfaces,²⁵ allow for the determination of G_{NW} in terms of the slopes s_1, s_2 [for Si(111) and Si(001), respectively], and s_{NW} defined in the linear elastic regime (Figure 5).

The radial indentation modulus M_{NW} has been computed via eq 5 and is listed in Table 1 for several nanowires with diameters below 150 nm. The table includes the radial Young's modulus E_{NW} , calculated in the isotropic approximation (eq 3) and using an average Poisson ratio of $\nu_{NW} = 0.3$. The lateral shear modulus G_{NW} is also given in Table 1. We have determined the same elastic moduli for ZnO nanobelts of large cross sections in order to have a clear idea of their bulk limits. Indeed, the Young's modulus found for the nanobelt compares well with the value of 112 GPa reported for single-crystal ZnO bulk oriented along [0001].²⁶ Our data show that the size effects for [0001] ZnO NWs are significant for wire diameters smaller than 80 nm. We have found that all three moduli (M_{NW} , E_{NW} , and G_{NW}) approximately double their values (with respect to the bulk limits) when the NW diameter is decreased to 25 nm (Table 1).

Table 1: The Radial Indentation Modulus M_{NW} , Young's Modulus E_{NW} , and Lateral Shear Modulus G_{NW} for Several ZnO NWs^a

NW diameter (nm)	M_{NW} (GPa)	E_{NW} (GPa)	G_{NW} (GPa)
25.5	217.5	198.0	109.4
36.2	170.0	154.7	97.5
36.6	170.4	155.1	98.0
46.0	122.6	111.5	
61.0	140.2	127.6	75.4
80.0	112.8	102.6	
134.4 nanobelt	114.6	104.3	50.7
	109.8	100.0	51

^a The elastic moduli have also been determined for a ZnO nanobelt with a 250 nm × 450 nm rectangular cross section (last row). The maximum uncertainty for each modulus is ±15.0 GPa.

The elastic moduli reported here are calculated using the sphere-on-cylinder (SOC) model^{7,27} for the contact between the tip and the ZnO NW, as opposed to the simpler and more widespread sphere-on-elastic halfspace (SOH) model. Despite the complexity of the SOC model, we argue that when the wire diameters are comparable to the diameter of the probe tip (as seen in Figure 3b), the SOC model has to be used since it necessarily yields more accurate and reliable elastic properties. A recalculation of the ZnO NW elastic moduli based on the simpler SOH geometry gives markedly different values than those in Table 1. Still, the results of the sphere-on-halfspace and sphere-on-cylinder analyses should obviously converge in the limit of thick nanowires. Indeed, the indentation modulus (114.6 GPa) for the largest wire computed using the SOC geometry is only slightly greater than the indentation modulus of the 250 nm × 450 nm nanobelt (~110 GPa), which was calculated using the SOH model.

The size dependence of the elastic properties of ZnO NWs can be understood qualitatively by recognizing that the thinner nanowires have a relatively larger number of atomic bonds in the surface and near-surface layers and that these bonds are shorter and stiffer than their bulk counterparts. This explanation is supported by density functional theory calculations²⁸ which consistently show that the interlayer distances and the bond lengths decrease for the relaxed ZnO(11 $\bar{2}$ 0) and ZnO(10 $\bar{1}$ 0) surfaces, which are both parallel to the wire orientation. A more quantitative approach stems from modeling the nanowire as a cylindrical core (bulk) and a shell (surface region) that have different radial elastic moduli E_c and E_s , respectively (for simplicity, we consider the Poisson ratio to have the same value of 0.3 in the core as it has in the shell). For a core-shell nanowire with a shell thickness t and a core radius $R_c \equiv R_{\text{NW}} - t$, a realistic estimate of the radial Young's modulus E_{NW} can be gained from the analysis of strain under conditions of uniform radial stress, which yields

$$\frac{R_{\text{NW}}}{E_{\text{NW}}} = \frac{t}{E_s} + \frac{R_c}{E_c} \quad (8)$$

The strain analysis for a NW subjected to a shear load

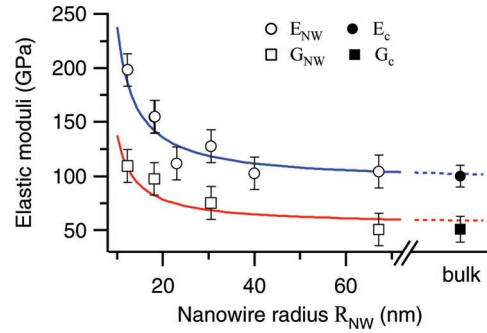


Figure 6. Elastic moduli E_{NW} and G_{NW} obtained from measurements (data points) and fitted as functions of the nanowire radius according to eq 8 for E_{NW} (blue curve) and eq 9 for G_{NW} (red curve).

distributed uniformly (for simplicity) on its lateral surface yields a similar equation for the shear modulus G_{NW}

$$\frac{R_{\text{NW}}}{G_{\text{NW}}} = \frac{t}{G_s} + \frac{R_c}{G_c} \quad (9)$$

Fitting the Young's modulus data from Table 1 to eq 8, we estimate the parameters of the core-shell model to be $E_c = 95$ GPa, $E_s = 190$ GPa, and $t = 12$ nm. The fit curve is depicted in Figure 6 and shows that in the bulk limit, the radial Young's modulus tends to the fitting parameter E_c . The value $t = 12$ nm is consistent with estimations of the shell thickness based on our HRTEM images (Figure 2c), which show a polycrystalline surface layer that is at least 5 nm thick. Interestingly, the shell thickness $t = 12$ nm that we have obtained is also in order-of-magnitude agreement with an independent assessment based on a core-shell model for the axial Young's modulus.⁴ Such assessment, which places the shell thickness at 4.4 nm,⁴ is the result of extracting the effective axial Young's modulus of the nanowire from the sum of the flexural rigidities of a core and a shell that have different axial moduli (E_c^{\parallel} and E_s^{\parallel} , respectively). We note that the core-shell analysis for the axial Young's modulus⁴ is not applicable for our experiments because the expressions of core-shell models for elastic properties of nanowires actually depend on the particular elastic property being analyzed and on the type of deformation to which the nanowire is subjected. However, for both the axial Young's modulus⁴ and the radial modulus presented here, suitably designed core-shell models appear to satisfactorily capture the increase of the corresponding elastic modulus with decreasing nanowire diameter.

With the shell thickness determined from fitting the E_{NW} values, we tested that the same parameter t was consistent with the shear modulus data. Using $t = 12$ nm in eq 9, the remaining fit parameters were found to be $G_c = G_s/2 = 55$ GPa. The fitting curve (eq 9) is also shown in Figure 6 and tends to the bulk limit value G_c when the wire radius increases. Therefore, the shell thickness ($t = 12$ nm) estimated from fitting the Young's modulus data is also consistent with a core-shell model that describes the shear modulus (eq 9).

A closer look at the parameters ($t = 12$ nm, $E_s = 2E_c = 190$ GPa) that we have found for our core–shell model (eq 8) and at the parameters reported in ref 4 for axial deformations ($t = 4.4$ nm, $E_s^{\parallel} = 1.5E_c^{\parallel} = 210$ GPa) shows that, in fact, both core–shell models remain somewhat qualitative because, in both of them, the thickness parameter ends up being the radius of the smallest nanowire investigated, and the value E_s closely corresponds to the thinnest nanowire. In neither of the models does the Young's modulus saturate at a constant E_s as the diameter is decreased past a certain value, which means that the fits only hold within the diameter range studied. The reason for this most probably lies in the fact that the models, while providing reasonable interpretation of the experimental data, are perhaps too simplified. The ZnO NWs in our experiments have a polycrystalline shell (Figure 2c) that cannot be in epitaxial relation with the core of the nanowire, which means that the stress created at the interface could effectively modify the elastic properties of the core. Even in the absence of a polycrystalline shell, the strain experienced by the surface layers due to reconstruction and relaxation depends on the diameter of ZnO NWs, and thus, the concept of a shell with constant elastic modulus may only hold as an approximation.

In conclusion, CR-AFM measurements analyzed in the framework of the Hertzian contact model are shown to provide insight into the radial elastic properties of nanowires in a versatile and nondestructive way. Similarly, friction-type measurements are useful to directly probe the effects of surface stiffening on the shear response of the nanowire. The approach presented here complements the arsenal of present methodologies of investigating the mechanical response of NWs in the following ways: (a) no macroscopic displacement of the wires (or segments thereof) is involved, (b) when nanowires are used as substrate-supported parts of piezoelectric or electromechanical devices, the investigations can be performed in situ, that is, by taking the substrate (as is) into the AFM, and (c) detection of defects in the NWs can be readily made by studying the elastic response at various locations on the wire surface. Using the above methodology for the particular case of ZnO NWs oriented along the [0001] direction, we have found that both the lateral shear modulus and radial indentation modulus increase significantly with decreasing nanowire diameter, which is due to a surface stiffening effect consistent with previous reports. A core–shell model of the nanowire suggests that these results could be understood by a competition between the elastic properties of the bulk core and those of a (stiffer) surface shell of roughly constant thickness, with the elastic properties of the shell becoming predominant in the limit of small ZnO NW diameters.

Acknowledgment. The authors would like to thank Kyle Sullivan (University of Maryland) and Albert Davydov (NIST) for the HRTEM and the SEM imaging.

References

- (1) (a) Xia, Y. N.; Yang, P. D.; Sun, Y. G.; Wu, Y. Y.; Mayers, B.; Gates, B.; Yin, Y. D.; Kim, F.; Yan, Y. Q. *Adv. Mater.* **2003**, *15*,

353. (b) Wang, Z. L. *J. Phys.: Condens. Matter* **2004**, *16*, R829. (c) Lu, W.; Lieber, C. M. *J. Phys. D: Appl. Phys.* **2006**, *39*, R387. (d) Wang, X. D.; Song, J. H.; Wang, Z. L. *J. Mater. Chem.* **2007**, *17*, 711.
- (2) (a) Yang, P. D.; Yan, H. Q.; Mao, S.; Russo, R.; Johnson, J.; Saykally, R.; Morris, N.; Pham, J.; He, R. R.; Choi, H. J. *Adv. Funct. Mater.* **2002**, *12*, 323. (b) Wang, Z. L. *Adv. Mater.* **2003**, *15*, 432. (c) Kong, X. Y.; Wang, Z. L. *Nano Lett.* **2003**, *3*, 1625. (d) Kong, X. Y.; Ding, Y.; Yang, R.; Wang, Z. L. *Science* **2004**, *303*, 1348. (e) Fan, Z. Y.; Lu, J. G. *J. Nanosci. Nanotechnol.* **2005**, *5*, 1561.
- (3) (a) Wang, Z. L.; Song, J. H. *Science* **2006**, *312*, 242. (b) Song, J. H.; Zhou, J.; Wang, Z. L. *Nano Lett.* **2006**, *6*, 1656. (c) Wang, Z. L. *Appl. Phys. A* **2007**, *88*, 7.
- (4) Chen, C. Q.; Shi, Y.; Zhang, Y. S.; Zhu, J.; Yan, Y. J. *Phys. Rev. Lett.* **2006**, *96*, 075505.
- (5) Huang, Y. H.; Bai, X. D.; Zhang, Y. J. *J. Phys.: Condens. Matter* **2006**, *18*, L179.
- (6) Bai, X. D.; Gao, P. X.; Wang, Z. L.; Wang, E. G. *Appl. Phys. Lett.* **2003**, *82*, 4806.
- (7) Feng, G.; Nix, W. D.; Yoon, Y.; Lee, C. J. *J. Appl. Phys.* **2006**, *99*, 074304.
- (8) Song, J. H.; Wang, X. D.; Riedo, E.; Wang, Z. L. *Nano Lett.* **2005**, *5*, 1954.
- (9) Ni, H.; Li, X. *Nanotechnology* **2006**, *17*, 3591.
- (10) Ji, L. W.; Young, S. J.; Fang, T. H.; Liu, C. H. *Appl. Phys. Lett.* **2007**, *90*, 033109.
- (11) Mai, W.; Wang, Z. L. *Appl. Phys. Lett.* **2006**, *89*, 073112.
- (12) Lucas, M.; Mai, W.; Yang, R.; Wang, Z. L.; Riedo, E. *Nano Lett.* **2007**, *7*, 1314.
- (13) (a) Rabe, U.; Janser, K.; Arnold, W. *Rev. Sci. Instrum.* **1996**, *67*, 3281. (b) Yamanaka, K.; Nakano, S. *Jpn. J. Appl. Phys.* **1996**, *35*, 3787.
- (14) (a) Lantz, M. A.; O'Shea, S. J.; Welland, M. E.; Johnson, K. L. *Phys. Rev. B* **1997**, *55*, 10776. (b) Carpick, R. W.; Ogletree, D. F.; Salmeron, M. *Phys. Rev. Lett.* **1997**, *70*, 1548. (c) Mate, C. M.; McClelland, G. M.; Erlandsson, R.; Chiang, S. *Phys. Rev. Lett.* **1987**, *59*, 1942.
- (15) (a) Heidelberg, A.; Ngo, L. T.; Wu, B.; Phillips, M. A.; Sharma, S.; Kamins, T. I.; Sader, J. E.; Boland, J. J. *Nano Lett* **2006**, *6*, 1101. (b) Xong, Q.; Duarte, N.; Tadigadapa, S.; Eklund, P. C. *Nano Lett.* **2006**, *6*, 1904.
- (16) Huang, M. H.; Wu, Y.; Feick, H.; Tran, N.; Weber, E.; Yang, P. *Adv. Mater.* **2001**, *13*, 113.
- (17) Liu, Y.-L.; Jian, W.-B.; Wang, C. P.; Suen, Y.-W.; Wu, Z.-Y.; Chen, F.-R.; Kai, J.-J.; Liu, J.-J. *Appl. Phys. Lett.* **2007**, *90*, 223117.
- (18) Liu, D. F.; Xiang, Y. J.; Zhang, Z. X.; Wang, J. X.; Gao, Y.; Song, L.; Liu, L. F.; Dou, X. Y.; Zhao, X. W.; Luo, S. D.; Wang, C. Y.; Zhou, W. Y. Z.; Wang, G.; Xie, S. S. *Nanotechnology* **2005**, *16*, 2665.
- (19) Certain commercial instruments or materials are identified here to adequately specify the experimental procedure. Such identification is not intended to imply recommendation or endorsement by the National Institute of Standards and Technology, nor is it intended to imply that the materials or equipment identified are necessarily the best available for the purpose.
- (20) (a) Burnham, N. A.; Chen, X.; Hodges, C. S.; Matei, G. A.; Thoreson, E. J.; Roberts, C. J.; Davies, M. C.; Tendler, S. J. B. *Nanotechnology* **2003**, *14*, 1. (b) Sader, J. E.; Chon, J. W. M.; Mulvaney, P. *Rev. Sci. Instrum.* **1999**, *70*, 3967.
- (21) Stan, G.; Price, W. *Rev. Sci. Instrum.* **2006**, *77*, 103707.
- (22) Gladwell, G. M. L. *Contact Problems in the Classical Theory of Elasticity*; Sijthoff & Noordhoff, Alphen aan den Rijn: The Netherlands, 1980.
- (23) Equations 8.111–8.112 from Gradshteyn, I. S.; Ryzhik, I. M. *Table of Integrals, Series and Products*, 6th ed.; Academic Press: New York, 2000.
- (24) Wortman, J. J.; Evans, R. A. *J. Appl. Phys.* **1965**, *36*, 153. The indentation modulus M_{ref} for Si(111) is evaluated as $E_{\text{ref}}/(1 - \nu_{\text{ref}}^2)$, where $E_{\text{ref}} = 187.5$ GPa is the Young's modulus along [111] and $\nu_{\text{ref}} = 0.18$ is the Poisson ratio that corresponds to [111] and to any direction within the (111) plane. Since the Si probe tip is oriented along [001], the modulus M_{T} is calculated accordingly using $E_{\text{T}} = 130.2$ GPa and $\nu_{\text{T}} = 0.28$.

- (25) Shear modulus values are required for the two chosen reference surfaces; these are given in ref 24 as 57.8 GPa for Si(111) and 79.4 GPa for Si(001).
- (26) Kucheyev, S. O.; Bradby, J. E.; Williams, J. S.; Jagadish, C.; Swain, M. V. *Appl. Phys. Lett.* **2002**, *80*, 956.
- (27) Palaci, I.; Fedrigo, S.; Brune, H.; Klinke, C.; Chen, M.; Riedo, E. *Phys. Rev. Lett.* **2005**, *94*, 175502. It is worth emphasizing that the modulated nanoindentation technique used by Palaci et al. for carbon nanotubes is different from CR-AFM. The modulated nanoindentation

uses a constant frequency while the force is modulated. In contrast, in CR-AFM, the modulation frequency is swept from 100 KHz to several MHz in order to find the resonances of the AFM probe in contact with the nanowire.

- (28) (a) Wander, A.; Harrison, N. M. *Surf. Sci.* **2000**, *457*, L342. (b) Wander, A.; Harrison, N. M. *Surf. Sci.* **2001**, *468*, L851.
- (29) Mindlin, R. D. *J. Appl. Mech.* **1949**, *16*, 269.

NL071986E